Theoretical Study on the Adsorption and Hydrogenation Mechanism of 2-Methylthiophene over the Pt(111) Catalyst

SHI Wei[(1)](施炜);NI Zhe-Ming[(2)](倪哲明);XIA Sheng-Jie[(2)](夏盛杰);SU Wei-Ke[(1)](苏为科)

[(1)] *National Engineering Research Center for Process Development of Active Pharmaceutical Ingredients, Collaborative Innovation Center of Yangtze River Delta Region Green Pharmaceuticals, Zhejiang University of Technology, Hangzhou* 310032, *China*);[(2)] *Laboratory of Advanced Catalytic Materials, College of Chemical Engineering, Zhejiang University of Technology, Hangzhou* 310032, *China*

ABSTRACT The adsorption process and hydrogenation mechanisms of 2-methylthiophene on the Pt(111) surface have been elucidated using density functional theory (DFT). The optimal adsorption sites of reactants, intermediates, and products as well as the activation energy and reaction energy of each elementary reactions were investigated. The results turned out that the 2-methylthiophene tilt to the Pt(111) catalyst with the C_1–C_2 double bond at the top site was the most stable. During the hydrogenation process, the heat of reaction almost located at the negative side, so dropping the temperature is good for the occurrence of hydrogenation process. The hydrogenation steps of mechanism take place along $C_2 \rightarrow C_3 \rightarrow C_1 \rightarrow C_4 \rightarrow S \rightarrow C_1$ to generate the product of pentane-2-thiol, in which the first step with the highest energy barrier is the rate-determining step.

Keywords: density functional theory; 2-methylthiophene; Pt(111), adsorption; hydrogenation mechanisms;

DOI: 10.14102/j.cnki.0254-5861.2011-1644

1 INTRODUCTION

In modern society, with the increasing consumption of energy demand along with the growing shortage of energy supply and the development of people's consciousness to curb greenhouse gas

emissions, many research efforts are focused on the exploitation of new types of energy resources[1-5].

Hydrogen is regarded as one of the high-performance, low cost and environmentally-friendly energy resource[6-8], which has been widely applied in the fields of electronics, petrochemical, metallurgy, machinery and so on[9-11]. However, owing to the storage restrictions of low energy density materials, there are still some limitations in the usage of hydrogen[12, 13]. As a result, plenty of hydrogen storage materials with high energy density were developed in the last three years[14-17].

2-Methylthiophene (2MT) is a group of representative heteroatom aromatic rings and the electron-donating effects of methyl favor hydrogen release both thermodynamically and kinetically under mild conditions[18, 19]. Besides, further cleavage of one of the C–S bond during the hydrogenation process can carry an additional mole of hydrogen. For these reasons, it is considered to be one of the effective materials for hydrogen storage. Celis-Cornejo *et al.*[20] investigated the adsorption of 2MT on the supported catalyst of CoMo/γ-Al_2O_3 during the hydrogenation process. They found that the adsorption mechanism is in accordance with the Langmuir-Hinshelwood model. Zhao *et al.*[19] compared 16 catalysts for hydrogenation and ring-opening of 2MT, finding that the catalyst of Pt exhibited the best reactivity and selectivity. Furthermore, they proposed the possible reaction equation of hydrogenation process. Although there are some researches on the hydrogenation of 2MT currently, the hydrogenation mechanism of the process is very few because of the limitations of characterization and the complexity of reaction.

Density functional theory (DFT)[21, 22] has become a unique and powerful research approach for examining individual elementary reaction steps at the molecular level. Gece[23] used DFT methods to find that thiophene has a considerable tendency for the protonation and the most probable site of protonation is the α-position. Zhu *et al*[24, 25] studied the most efficient hydrogenation route of thiophene on different crystal planes of Pt catalyst. Our previous theoretical calculations[26-28] have been performed to investigate the adsorption and hydrogenation process of thiophene catalyzed on Au, Pd and Au/Pd catalysts in order to study the most favourable pathway for thiophene hydride sulfurization.

Despite these efforts mentioned above, as far as we know, no theoretical reports are available to

show the adsorption behavior and hydrogenation process of 2MT on the Pt catalyst. So in this study, Dmol^3 program package of DFT method was used to calculate the hydrogenation storage of 2MT and its hydrogenated derivatives on clean Pt(111) surface. The aim of this study is to analyze the possible hydrogenation storage pathways of 2MT and further to make better sense of Pt catalysts at the molecular level for the hydrogenation of 2MT.

2 COMPUTATIONAL METHODS AND MODEL

2. 1 Methods

All DFT simulations were conducted using the Dmol^3 program package[29] in the Materials Studio 6.0 of Accelrys Inc. In the whole study, the Perdew and Wang (PW91)[30-32] function with the generalized gradient approximation (GGA) was adopt. The double numerical basis set with polarization functions (DNP) was employed to describe the valence atomic orbitals. The convergence criterion of energy, maximum force, maximum displacement and maximum self-consistent-field (SCF) were set as 5×10^{-5} eV, 2×10^{-2} eV/nm, 5×10^{-4} nm, and 2×10^{-5} eV/atom respectively. Furthermore, the transition states (TS) from reactants and products were searched by means of complete LST (linear synchronous transit)/QST (quadratic synchronous transit) method[33]. The calculated TS was confirmed by the fact that the structure possesses only one imaginary vibration frequency and the vibrational vector for this imaginary frequency is along the reaction direction. During computation, the Fermi smearing method is employed to determine electron occupancies with a smearing width of 0.1 eV.

2. 2 Catalyst model

Based on the optimized structure of Pt bulk, we built up a four-layer Pt(111) surface with a (4 × 4) unit cell (64 Pt atoms in a cell), which corresponds to 1/16 monolayer (ML) for a single 2MT on the surface, as shown in Fig. 1. The reciprocal space was sampled with a (5 × 5 × 1) k-points grid generated automatically using the Monkhorst-Pack method and the vacuum region thickness of 1 nm was added into the perpendicular direction to prevent the interactions from various periodic configurations. It created a unit in the space by making use of the layer and the vacuum region repeated. During the geometry optimization and TS search, the bottom bilayer for Pt(111) was kept fixed during calculations, while the rest atoms were allowed to move freely. With the

parameters presented above, the calculated lattice constant for the Pt(111) surface was 0.3924 nm, which is consistent with the experimental data of 0.3923 nm[34, 35]. The results of simulating calculation show that the method used in this paper is correct and feasible.

3 RESULTS AND DISCUSSION

3. 1 Adsorption

Calculation of the adsorption energies is always regarded as an efficient measure, which can be used to illustrate the transform of the adsorbate-substrate before and after adsorption. In this work, the adsorption energy (E_{ads}) is defined as follows:

$$E_{ads} = E_{(A/surface)} - (E_A + E_{surface})$$

Where $E_{(A/surface)}$ is the total energy of 2MT together with the Pt(111) surface, E_A is the total energy of free 2MT molecule and $E_{surface}$ is the total energy of bare surface. By this definition, the more negative values of adsorption energy denote the more stable binding between the 2MT molecule and the Pt(111) surface.

According to the structure of ring-plane of 2MT and the results that we had been concluded[26-28, 36], 2MT adsorbed in the parallel direction to the Pt(111) surface is considered to be more stable than in the vertical direction. For this reason, the sixteen possible parallel adsorption sites are labeled by local coordination: (1) four top sites (0 °, 30 °, 60 °, 90 °), (2) four hcp sites (0 °, 30 °, 60 °, 90 °), (3) four fcc sites (0 °, 30 °, 60 °, 90 °) and (4) four bridge sites (0 °, 30 °, 60 °, 90 °), as shown in Fig. 1. Different angles in Fig. 1 represent 2MT rotating 0 °, 30 °, 60 °and 90 °around the symmetry axis of ring-plane from the horizontal.

Table 1 summarizes the calculated adsorption energies of 2MT adsorbed on the Pt(111) surface. In Table 1, the data of adsorption energies are divided into two parts with the energy around –139.0 and –175.0 kJ·mol^{-1}. The molecule of 2MT preferred to adsorb in a tilted way through the double bond which is far away from the functional group of methyl. Among different initial positions, 2MT adsorbed on the site of Top-60 °with the lowest E_{ads} of –175.0 kJ·mol^{-1} is regarded as the most stable configuration. Additionally, the top and side views of the most stable structure of 2MT adsorbed on the Top-60 °site are shown in Fig. 2.

In Fig. 2, the ring-plane spins clockwise around the axial; meanwhile, the methyl associated

with the double bond of C_3 and C_4 moves away from the Pt(111) surface during the adsorption process. Finally, 2MT adsorbs on the bridge site via C_1–C_2 double bond. Table 2 lists the calculated structural parameters of the most stable adsorption site of 2MT on the Pt(111) surface. By making a result comparison in Table 2, the calculation bond length of 2MT also agrees well with the experimental data[37]. These phenomena suggest that our method in this study is suitable for the adsorption of 2MT on the Pt(111) catalyst. Furthermore, the bond length of d_2 has the biggest change, suggesting that the double bond of C_1 and C_2 is the probable site for the beginning of the reaction.

3. 2 Hydrogenation mechanism of 2MT

On the basis of our previous research results[19], the product of hydrogenation was classified into two types of thiols on the Pt catalyst in the reaction process. Fig. 3 lists the structures of all intermediates in sequence of the hydrogenation process of 2MT.

We simulated the optimal configuration of reactants (IS), products (FS) and corresponding transition states (TS) in Fig. 3. The activation energies and reaction energies at TS are tabulated in Table 3. Based on the different hydrogenation pathways, we regarded the co-adsorption of 2MT and hydrogen as the first step, and then made a comparison of intermediate steps (steps 1～5 in Fig. 3).

3. 2. 1 IS1* + H* → C_5H_7S* (FS1～4)

At the start of reaction, we considered the initial product of hydrogenation storage exhibits four different possibilities, including FS1～FS4. The calculated barriers (E_a), the total energy change (ΔE), and the corresponding structures of IS, TS and FS in the mechanisms of step 1 are shown in Fig. 4. According to our calculations, the approach of H atom shifted to the bridge site from the adjacent fcc site and the 2MT still adsorbed on the bridge site via the C_1–C_2 double bond.

The product of FS1 moved to the left side in the horizontal direction; Meanwhile, the functional group of C_1–H tilted upward to be perpendicular to the Pt(111) surface and the atom C_4 shifted downward. Finally, the FS1 adsorbed on hollow site via the C_3–C_4 double bond. The TS1 was also calculated between IS1 and FS1 in Fig. 4. When the reaction was carried out, the atom H transferred to the fcc site and the atom C_1 moved downward slightly to form the C_1–H bond. The first step for the formation of FS1 was exothermic with ΔE of –52.2 kJ·mol^{-1} and the corresponding E_a was 167.7 kJ·mol^{-1}.

The functional group of C_2–H in FS2 tilted upward and the S atom as well as methyl moved downward. Therefore, the FS2 preferred to adsorb at the top site of Pt surface via S. During the formation of FS2, the H gradually shifted to the fcc site to get close to C_2 for the formation of methylene of C_2–H in TS2. The generation of FS2 was exothermic with ΔE of –8.1 kJ·mol^{-1} and the corresponding E_a to be 75.0 kJ·mol^{-1}.

The methyl of 2MT in FS3 tilted upward and was almost vertical to the Pt surface, and at the same time, the atom of C_3 shifted downward slightly to approach the surface. The FS3 adsorbed on the hollow site via the C_1–C_2 double bond was the most stable configuration. In TS3, the H atom moved to the top site, while the functional group of methyl was folded upward. The formation of FS3 was exothermic with ΔE of –54.9 kJ·mol^{-1} and the corresponding E_a was 130.9 kJ·mol^{-1}.

The molecule of FS4 almost has no change as compared to IS1 when the reaction happened. Finally, FS4 adsorbed on bridge site via the C_1–C_2 double bond. In TS4, the atom H moved away from the Pt surface to the adjacent fcc site to approach C_3. These phenomena are conductive to the formation of another bond of C_3–H. The formation of FS4 was endothermic with ΔE of 29.7 kJ·mol^{-1} and the corresponding E_a of 187.1 kJ·mol^{-1}.

It can be made a comparison among FS1, FS3 and FS4 from Table 3 and Fig. 4. The activation energy of FS2 is minimum, which indicates that the formation of FS2 is more likely to generate in step 1. This result is consistent with the analysis of the structure parameters in 2MT. Thermodynamically, the relative energy of FS1～FS3 is exothermic with a negative value. Reducing the temperature can improve the hydrogenation reactions. In contrast, the relative energy of FS4 is endothermic with positive value, so higher temperature is helpful for the hydrogenation reactions.

3. 2. 2 IS2* + H*→C_5H_8S* (FS5～FS7)

FS2 is identified as the dominant product in the first step, and further hydrogenation process of step 2 has three possible products: FS5 or FS6 or FS7. The E_a, ΔE, and the corresponding structures of IS, TS and FS of step 2 are shown in Fig. 5. It is observed that step 2 begins with the co-adsorption of FS2 and H. The FS2 adsorbed on the top site via the S and H atoms moved to the bridge site when the co-adsorption happened.

For the product of FS5, its S atom shifted downward to the Pt surface and the reacted methyne

tilted upward to relieve the steric hindrance for the H atom. Ultimately, the FS5 adsorbed on the top site of Pt surface through the S atom. In TS5, the H atom shifted to the hollow site to get close to the reacted α-C, finally forming a new C_1–H bond. The formation of FS5 was endothermic with ΔE of 11.6 kJ·mol^{-1} and the corresponding E_a to be 164.6 kJ·mol^{-1}.

For the product of FS6, we can see that the methyl moved upward slightly and its product still adsorbed on the top site through the S atom. Moreover, we optimize the configuration of TS6, as shown in Fig. 5. The atom H shifted away from the surface to approach C_3 to form another bond of C_3–H, while the distance between H and C_3 reduced from 0.4215 to 0.2644 nm. The formation of FS6 was endothermic with ΔE of 5.3 kJ·mol^{-1} and the corresponding E_a was 19.5 kJ·mol^{-1}.

For product FS7, the atoms of C_1-C_4 located closely to the surface and the methyl migrated upward to be perpendicular to the surface due to the attack of H atom. At last, FS7 adsorbed on the top site through atom S. In TS7, the atom H shifted from the bridge site to the fcc site and the relevant C_4–H distance was reduced to 0.5057 nm from 0.2458 nm in IS2. The formation of FS7 is endothermic: ΔE = 76.4 kJ·mol^{-1} and E_a = 109.3 kJ·mol^{-1}.

As shown in Table 3 and Fig. 5, the relative energy of FS5-FS7 was endothermic with positive value, so raising the temperature was benefit for the second step of hydrogenation reaction. Moreover, the relative energy as well as the reaction energy of FS6 is the lowest among the different products. These phenomena implied that the process to FS6 from IS2 was more likely to happen in step 2.

3. 2. 3 IS3* + H*→C_5H_9S* (FS8 or FS9)

In step 2, FS6 was deemed as the dominant product, which would further hydrogenate to form FS8 or FS9. The activation and reaction energies of IS, TS and FS in the mechanisms of step 3 are illustrated in Fig. 6. It begins from the most favorable co-adsorption configuration of FS6 and the H atom. Through optimization, the H atom shifted away from fcc site to the bridge site and the FS6 adsorbed on hollow site through the S atom.

The product of FS8 transferred to the bottom right and the atoms of C_1–C_4 shifted away from the Pt surface. Meanwhile, the atom C_5 moved downward to make the bond of C_4–C_5 parallel to the surface. Finally, the FS8 adsorbed on the top site through the atom S. In TS8, the atom H migrated to get close to the atom of C_1 and the relevant C_1–H distance was reduced to 0.3581 nm from 0.4911 nm in the IS3. The formation of FS8 was exothermic with ΔE of –102.1 kJ·mol^{-1} and

the corresponding E_a was 67.9 kJ·mol^{-1}.

During the process of IS3-FS9, there was a significant distortion in atoms C_2 and C_3. The FS9 adsorbed on the top site via the S atom is the most stable configuration. The H atom shifted to the adjacent hollow site, while the methylene of C_2 and C_3 tilted up, as shown in TS9. The formation of FS9 was endothermic with ΔE of 5.3 kJ·mol^{-1} and the corresponding E_a was 97.3 kJ·mol^{-1}.

According to the above results of simulations, IS3 prefers to hydrogenate on α-C_1 rather than α-C_2. The generation of FS8 is exothermic, while that of FS9 is endothermic. In addition, a lower barrier of 67.9 kJ·mol^{-1} along with a shorter bond length is present for the α-C_1–H bond formed in FS8. Consequently, the hydrogenation of IS3 to FS8 is likely to occur.

3. 2. 4 IS4* + H*→$C_5H_{10}S$* (FS10)

From previous discussion in step 3, the FS8 is identified as the most optimal product. There is only one kind of possible pathway for further hydrogenation of FS8 to form the saturate production of $C_5H_{10}S$. The activation and reaction energies of IS, TS and FS in the mechanisms of step 4 are shown in Fig. 7. It can be perceived that the initial hydrogenation channel of step 4 was the co-adsorption of FS8 and atom H. After co-adsorption, the H atom located at the bridge site and the FS8 kept almost the same structure, as compared in step 4.

The product of FS10 slanted towards the Pt(111) surface through the atom S, and at the same time, the functional group of methyl tilted upward to decrease the steric hindrance of the reaction. In TS10, the H atom transferred to the adjacent top site to approach the atom of C_4 and finally a new bond of C_1–H was formed. The formation of FS10 was exothermic with ΔE of –97.0 kJ·mol^{-1} and the corresponding E_a was 112.6 kJ·mol^{-1}.

3. 2. 5 IS5* + H*→$C_5H_{11}S$* (FS11～FS14)

In step 5, FS10 is further hydrogenated to thiol by the help of H atom. The activation and reaction energies of IS, TS and FS in the mechanisms of step 5 are shown in Fig. 8. The hydrogenation began with the FS10 locating at top site on the Pt(111) surface through the atom S and the H atom moved from fcc site to the top site.

The atoms of C_2-C_5 in FS11 tilted upward and distorted hugely. At the same time, the atoms of C_1 and S moved downward, which made FS11 adsorb on the Pt surface stably. In TS11, the distance between the H and S atoms reduced from 0.3600 to 0.2500 nm. This phenomenon caused the bond of d_1 to break, which was accompanied by the shift of H atom to the adjacent top site and

downward shift of S atom, respectively. The formation of FS11 was endothermic with ΔE of 48.9 kJ·mol^{-1} and the corresponding E_a was 116.9 kJ·mol^{-1}.

The methyl of C_1 in FS12 shifted to the hcp site and the bonds of C_2 to C_5 kept in a straight line from top view. Finally, the FS12 adsorbed on top site through atom S. In TS12, the atom H moved to the adjacent bridge site and the bond of C_2 and C_3 rotated clockwise to get close with the attacking H atom. The forming distance of α-C–H reduced from 0.2770 to 0.2065 nm. The formation of FS12 was endothermic with ΔE of 39.3 kJ·mol^{-1} and the corresponding E_a was 388.2 kJ·mol^{-1}.

The molecule of FS13 rotated anticlockwise. Meanwhile, atoms C_3-C_5 tilted upward to keep away from the Pt surface. For these reasons, the FS13 adsorbed on top site through atom S. The TS13 was also calculated between IS5 and FS13 in Fig. 8. The atom H shifted to the adjacent fcc site to get close to the S atom, resulting in a decrease of distance between atoms S and H from 0.3600 to 0.1970 nm. The formation of FS13 was endothermic with ΔE of 138.3 kJ·mol^{-1} and the corresponding E_a was 233.9 kJ·mol^{-1}.

There was a huge distortion in the product of FS14, when the reaction occurred. The methyl rotated anticlockwise based on the atom of C_4 and the C_2–C_4 bond was folded up. In TS14, the H atom moved to bridge site to get close to C_4 to generate the bond of C_4–H, while the distance between dissociative H and C_4 reduced from 0.4582 to 0.2987 nm. The formation of FS14 was endothermic with ΔE of 13.0 kJ·mol^{-1} and the corresponding E_a was 416.0 kJ·mol^{-1}.

Through a comparative analysis of the calculation results of IS, TS and FS in Fig. 8, we can see the reaction energy of FS11 is 116.9 kJ·mol^{-1}, which was the smallest among FS11-FS14. Moreover, the relative energy of different products in step 5 was positive, thus high temperature was beneficial to improve the reaction. Based on the kinetic and thermodynamic opinions, the hydrogenation of FS10 on Pt surface is more likely to produce FS11 rather than FS12～FS14. These phenomena suggest that FS11 is more competitive in step 5.

3. 2. 6 IS6* + H*→$C_5H_{12}S$* (FS15)

The FS11 is the dominant product in step 5. Fig. 9 illustrates the activation and reaction energies of IS, TS and FS in the final step of hydrogenation process. The hydrogenation began with the co-adsorption of FS11 and H atom. When step 6 started, the H atom shifted to top site and the structure of $C_5H_{11}S$ remained the same as FS11.

For the final product of FS15, the molecule twisted like a shape from the top view and adsorbed at the top site via the S atom. For the intermediate of TS15, the methyl of C_1 moved upward, and at the same time, the atom H shifted to the adjacent hollow site to get close to C_1, while the distance between atoms H and C_1 reduced from 0.3017 to 0.2460 nm. The formation of FS15 was exothermic with ΔE of –15.8 kJ·mol^{-1} and the corresponding E_a was 210.8 kJ·mol^{-1}.

3. 3 Brief summary about hydrogenation process of 2MT

In this study, possible pathways involved in the hydrogenation mechanism of 2MT were investigated. The landscape of potential energy surface (PES) for each step is shown in Fig. 10. As Fig. 10 shows, the most favorable hydrogenation mechanism follows the steps as below: the 2MT was hydrogenated to FS2 which then underwent a second hydrogenation to yield FS6. The FS6 can further be hydrogenated to generate FS8. Then FS8 underwent hydrogenation to form FS10 which can undergo a fourth hydrogenation to produce FS11. Finally, the FS11 can be hydrogenated to generate pentane-2-thiol (FS15). These results are in agreement with the previous experimental studies in the literature[19]. During the different steps in Fig. 10, the first hydrogen step to generate FS1 was the rate-determining step.

4 CONCLUSION

We have investigated and compared the adsorption and hydrogenation mechanisms of 2-methylthiophene using periodic density functional theory method. Various adsorption modes of the intermediates involved in the reaction were studied from the energetic and geometrical viewpoints, and the hydrogenation mechanism has been clarified. The major findings can be summarized as follows.

Our calculations show that the tilt adsorption of 2MT at the top site through the C_1–C_2 double bond is the most stable. With the increase of bond length of 2MT after the adsorption happened, the atom H will most likely to attack the double bond of C_1 and C_2 of 2MT.

The dominant mechanism of hydrogenation process follows the steps of $C_2 \rightarrow C_3 \rightarrow C_1 \rightarrow C_4 \rightarrow S \rightarrow C_1$ to generate pentane-2-thiol from the view of dynamics. The hydrogenation process of 2MT is almost exothermic, so that dropping the temperature is beneficial for the hydrogenation process. In addition, the first step of hydrogenation of 2MT with the highest

activation barrier is the rate-determining step.

REFERENCES

(1) Konda, S. K.; Chen, A. C. Palladium based nanomaterials for enhanced hydrogen spillover and storage. *Mater. Today* **2016**, 19, 100–108.

(2) Zhang, Q.; Zheng, D. D.; Xu, L. S.; Chang, C. T. Photocatalytic conversion of terephthalic acid preparation wastewater to hydrogen by graphene-modified TiO_2. *Catal. Today* **2016**, 274, 8–14.

(3) Contreras, M. L.; Villarroel, I.; Rozas, R. Hydrogen physisorption energies for bumpy, saturated, nitrogen-doped single-walled carbon nanotubes. *Struct. Chem.* **2016**, 27, 1–12.

(4) Li, X. D.; Zhang, H.; Miyamoto, Y.; Tang, Y. J.; Wang, C. Y. Computational design of tetrahedral silsesquioxane-based porous frameworks with diamond-like structure as hydrogen storage materials. *Struct. Chem.* **2014**, 25, 177–185.

(5) Jiang, H.; Cheng, X. L.; Zhang, H.; Tang, Y. J.; Wang, J. Molecular dynamic investigations of hydrogen storage efficiency of graphene. *Struct. Chem.* **2015**, 26, 531–537.

(6) Toklu, E.; Avci, A. C.; Kaygusuz, K.; Gur, M. A research on hydrogen production from industrial waste heat by thermal water splitting. *Int. J. Hydrogen. Energ.* **2016**, 41, 10071–10079.

(7) Hosseini, S. E.; Wahid, M. A. Hydrogen production from renewable and sustainable energy resources: promising green energy carrier for clean development. *Renew. Sust. Energ. Rev.* **2016**, 57, 850–866.

(8) Ren, J.; Zhang, N. C.; Zhang, H.; Peng, X. J. First-principles study of hydrogen storage on Pt (Pd)-doped boron nitride sheet. *Struct. Chem.* **2015**, 26, 731–738.

(9) Iulianelli, A.; Liguori, S.; Huang, S.; Basile, A. Model biogas steam reforming in a thin Pd-supported membrane reactor to generate clean hydrogen for fuel cells. *J. Power. Sour.* **2015**, 273, 25–32.

(10) Moradi, M.; Naderi, N. First principle study of hydrogen storage on the graphene-like aluminum nitride nanosheet. *Struct. Chem.* **2014**, 25, 1289–1296.

(11) Zhang, S. L.; Feng, Y.; Zhang, D.; Jiang, Y. G.; Qin, J.; Bao, W. Parametric numerical analysis of regenerative cooling in hydrogen fueled scramjet engines. *Int. J. Hydrogen. Energ.* **2016**, 41, 10942–10960.

(12) Mazzucco, A.; Dornheim, M.; Sloth, M.; Jensen, T. R.; Jensen, J. O.; Rokni, M. Bed geometries, fueling strategies and optimization of heat exchanger designs in metal hydride storage systems for automotive applications: a review. *Int. J. Hydrogen. Energ.* **2014**, 39, 17054–17074.

(13) Zhang, Z. H.; Hu, C. System design and control strategy of the vehicles using hydrogen energy. *Int. J. Hydrogen. Energ.* **2014**, 39, 12973–12979.

(14) Shafiee, S.; McCay, M. H. Different reactor and heat exchanger configurations for metal hydride hydrogen storage systems-a review. *Int. J. Hydrogen. Energ.* **2016**, 41, 9462–9470.

(15) Niaz, S.; Manzoor, T.; Pandith, A. H. Hydrogen storage: materials, methods and perspectives. *Renew. Sust. Energ. Rev.* **2015**, 50, 457–469.

(16) Liu, W.; Webb, C. J.; Gray, E. M. Review of hydrogen storage in AB_3 alloys targeting stationary fuel cell applications. *Int. J. Hydrogen. Energ.* **2016**, 41, 3485–3507.

(17) Sun, W. P.; Zhang, Y.; Zhu, Y. F.; Zhuang, X. Y.; Dong, J.; Qu, Y.; Guo, X. L.; Chen, J.; Wang, Z. M.; Li, L. Q. The hydrogen storage performance of a $4MgH_2$-$LiAlH_4$-TiH_2 composite system. *J. Alloy. Compd.* **2016**, 676, 557–564.

(18) Song, X. L.; Fanelli, M. G.; Cook, J. M.; Bai, F. R.; Parish, C. A. Mechanisms for the reaction of thiophene and methylthiophene with singlet and triplet molecular oxygen. *J. Phys. Chem. A* **2012**, 116, 4934–4946.

(19) Zhao, H. Y.; Oyama, S. T.; Naeemi, E. D. Hydrogen storage using heterocyclic compounds: the hydrogenation of 2-methylthiophene. *Catal. Today* **2010**, 149, 172–184.

(20) Celis-Cornejo, C. M.; Granados-Zarta, G. A.; Bravo-Villarreal, C. E.; Perez-Martinez, D. D.; Giraldo-Duarte, S. A. Kinetic parameters determination of fcc gasoline hydrotreating using genetic algorithms. *CT. F-Cienc. Tecn. Fut.* **2016**, 5, 79–93.

(21) Heermann, D. W. *Computer Simulation Methods in Theoretical Physics*. Springer-Verlag Pres **1990**.

(22) Leach, A. R. *Molecular Modelling: Principles and Applications*. Addison Wesley Longman Limited Press **2001**.

(23) Gece, G. Theoretical evaluation of the inhibition properties of two thiophene derivatives on corrosion of carbon steel in acidic media. *Mater. Corros.* **2013**, 64, 940–944.

(24) Zhu, H. Y.; Lu, X. Q.; Guo, W. Y.; Li, L. F.; Zhao, L. M.; Shan, H. H. Theoretical insight into the desulfurization of thiophene on Pt(110): a density functional investigation. *J. Mol. Catal. A-Chem.* **2012**, 363–364, 18–25.

(25) Zhu, H. Y.; Guo, W. Y.; Li, M.; Zhao, L. M.; Li, S. R.; Li, Y.; Lu, X. Q.; Shan, H. H. Density functional theory study of the

adsorption and desulfurization of thiophene and its hydrogenated derivatives on Pt(111): Implication for the mechanism of hydrodesulfurization over noble metal catalysts. *Acs. Catal*. **2011**, 11, 1498–1510.

(26) Zhang, L. Y.; Shi, W.; Xia, S. J.; Ni, Z. M. Hydrodesulfurization mechanisms of thiophene catalyzed by Au/Pd(111) bimetallic surface. *Acta. Phys-Chim. Sin*. **2014**, 30, 1847–1854.

(27) Ni, Z. M.; Shi, W.; Xia, M. Y.; Xue, J. L. Theoretical studies on reaction mechanism of hydrodesulfurization of thiophene catalyzed by Au(111) plane. *Chem. J. Chin. U* **2013**, 34, 2353–2362.

(28) Shi, W.; Zhang, L. Y.; Ni, Z. M.; Xia, S. J.; Xiao, X. C. DFT investigations of the adsorption and hydrodesulfurization mechanism of thiophene catalyzed by Pd(111) surface. *RSC. Adv*. **2014**, 4, 58315–58324.

(29) Delley, B. From molecules to solids with the DMol^3 approach. *J. Chem. Phys*. **2000**, 113, 7756–7764.

(30) Perdew, J. P.; Chevary, J. A.; Vosko, S. H.; Jackson, K. A.; Pederson, M. R.; Singh, D. J.; Fiolhais, C. Atoms, molecules, solids, and surfaces-applications of the generalized gradient approximation for exchange and correlation. *Phys. Rev. B* **1992**, 46, 6671–6687.

(31) White, J. A.; Bird, D. M.; Payne, M. C.; Stich, I. Surface corrugation in the dissociative adsorption of H_2 on Cu(100). *Phys. Rev. Lett.* **1994**, 73, 1404–1407.

(32) Perdew, J. P.; Wang, Y. Accurate and simple analytic representation of the electron-gas correlation-energy. *Phys. Rev. B* **1992**, 45, 13244–13249.

(33) Halgren, T. A.; Lipscomb, W. N. The synchronous-transit method for determining reaction pathways and locating molecular transition states. *Phys. Lett.* **1977**, 49, 225–232.

(34) Kittel, C. *Solid State Physics*. John Wiley & Sons Press **1976**.

(35) Mai, S. W.; Zhou, G. D.; Li, W. J. *Advanced Inorganic Structural Chemistry*. Peking University Press **2001**.

(36) Chen, Z. H.; Ding, K. N.; Xu, X. L.; Li, J. Q. DFT study of thiophene adsorption on the Pd(111) and Pt(111) surfaces. *Chin. J. Struct. Chem*. **2010**, 29, 365–376.

(37) Tanabe, M.; Kuze, N.; Fujiwara, H.; Takeuchi, H.; Konaka, S. Molecular structure of 2-methylthiophene studied by gas electron diffraction combined with microwave spectroscopic data. *J. Mol. Struct*. **1995**, 372, 173–180.

Table 1. Adsorption Energies of 2MT on the Pt(111) Surface

Adsorption site	E_{ads} (kJ·mol^{-1})	Adsorption site	E_{ads} (kJ·mol^{-1})
Top-0 °	–140.7	Fcc-0 °	–171.9
Top-30 °	–140.4	Fcc-30 °	–167.6
Top-60 °	–175.0	Fcc-60 °	–140.3
Top-90 °	–174.2	Fcc-90 °	–139.8
Hcp-0 °	–141.0	Bri-0 °	–173.6
Hcp-30 °	–168.2	Bri-30 °	–170.8
Hcp-60 °	–140.3	Bri-60 °	–168.2
Hcp-90 °	–167.0	Bri-90 °	–139.4

The adsorption positions in Table 1 represent the initial adsorption sites of 2MT

Table 2. Adsorption Energy and Bond Lengths of 2MT Molecule on Pt(111) for the Most Stable Adsorption Geometry

Model	E_{ads} (kJ·mol^{-1})	d_1/nm	d_2/nm	d_3/nm	d_4/nm	d_5/nm	d_6/nm
2MT (Expt)[37]		0.1729	0.1371	0.1432	0.1374	0.1722	0.1505
2MT (Calc.)		0.1731	0.1370	0.1422	0.1375	0.1743	0.1495
2MT/Pt(111)	–175.0	0.1848	0.1507	0.1460	0.1356	0.1795	0.1484
$\|\Delta d\|$		0.0117	0.0137	0.0038	0.0019	0.0052	0.0011

Table 3. Activation Energy (E_a) and Reaction Energy (ΔE) of Elementary Reactions on the Pt(111) Surface

Reaction	E_a (kJ·mol^{-1})	ΔE (kJ·mol^{-1})

$C_5H_6S^* + H^* \rightarrow FS1^* + *$	167.7	–52.2
$C_5H_6S^* + H^* \rightarrow FS2^* + *$	75.0	–8.1
$C_5H_6S^* + H^* \rightarrow FS3^* + *$	130.9	–54.9
$C_5H_6S^* + H^* \rightarrow FS4^* + *$	187.1	29.7
$FS2^* + H^* \rightarrow FS5^* + *$	164.6	11.6
$FS2^* + H^* \rightarrow FS6^* + *$	19.5	5.3
$FS2^* + H^* \rightarrow FS7^* + *$	109.3	76.4
$FS6^* + H^* \rightarrow FS8^* + *$	67.9	–102.1
$FS6^* + H^* \rightarrow FS9^* + *$	97.3	5.3
$FS9^* + H^* \rightarrow FS10^* + *$	112.6	–97.0
$FS10^* + H^* \rightarrow FS11^* + *$	116.9	48.9
$FS10^* + H^* \rightarrow FS12^* + *$	388.2	39.3
$FS10^* + H^* \rightarrow FS13^* + *$	233.9	138.3
$FS10^* + H^* \rightarrow FS14^* + *$	416.0	13.0
$FS10^* + H^* \rightarrow FS15^* + *$	210.8	–15.8

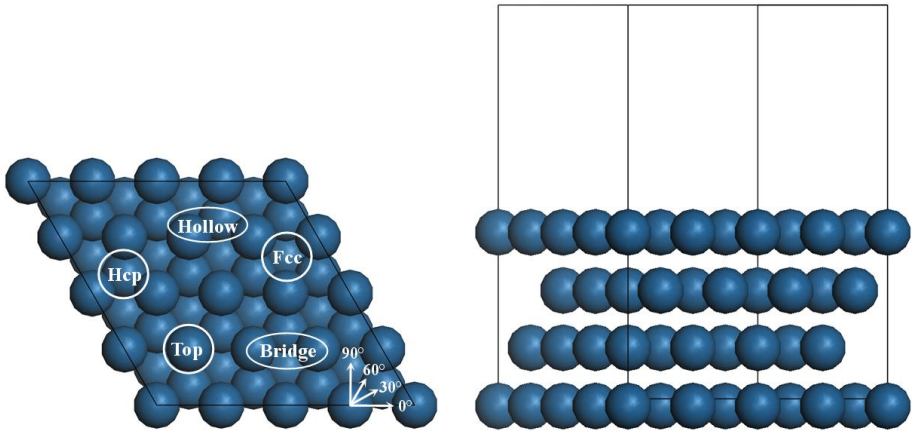

Fig. 1. Top (left) and side (right) view of Pt(111) surface models (4×4)

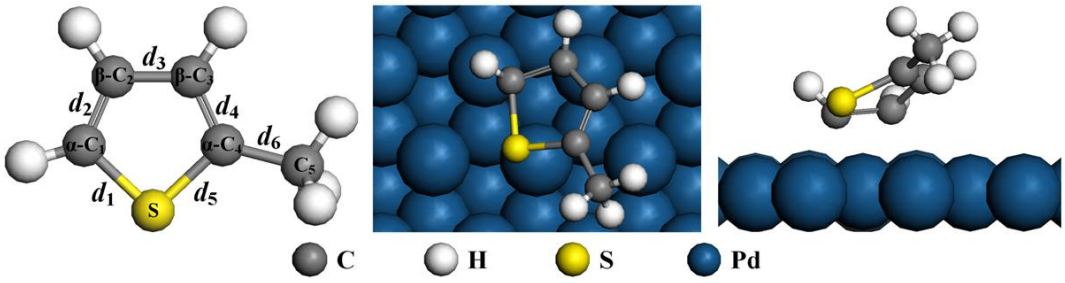

Fig. 2. The most stable configurations of 2MT on the Pt(111) surface

(a) represents 2MT; (b) represents top view; (c) represents side view

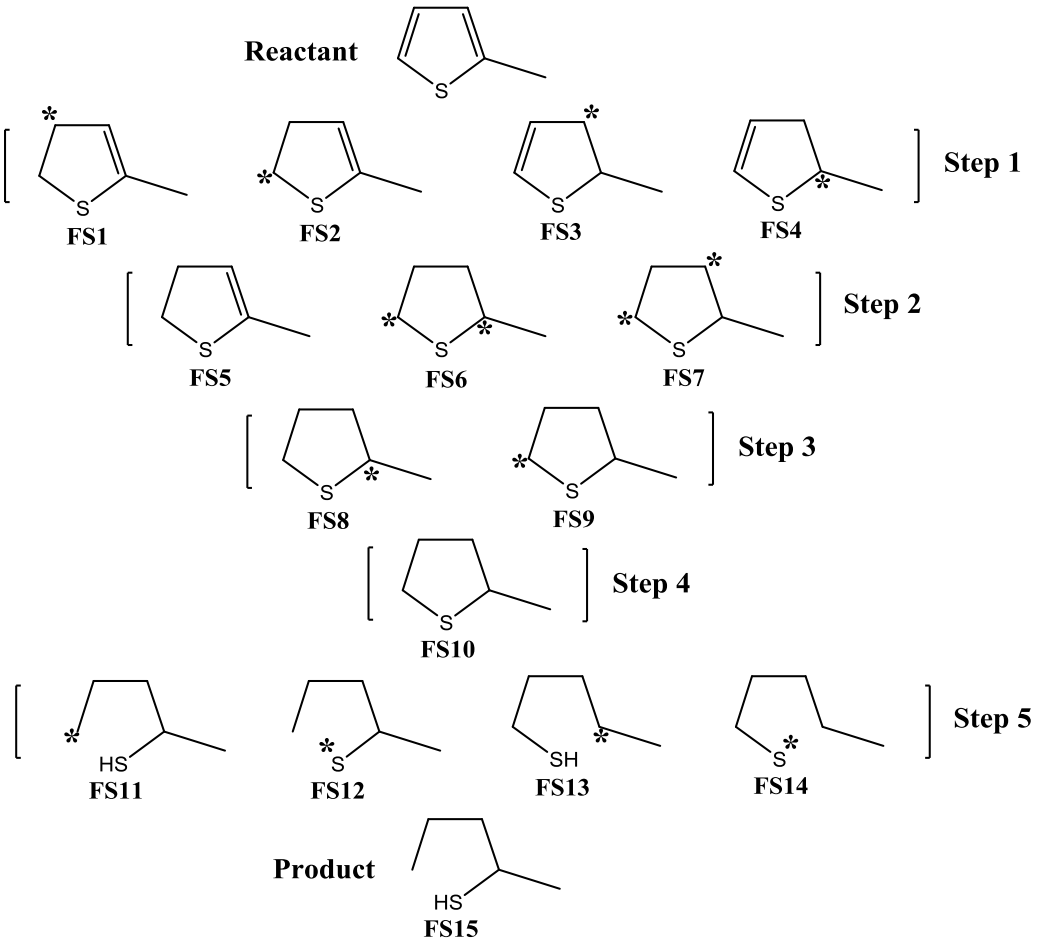

Fig. 3. Different reaction pathways for the hydrogenation storage of 2MT.

FS represents the product

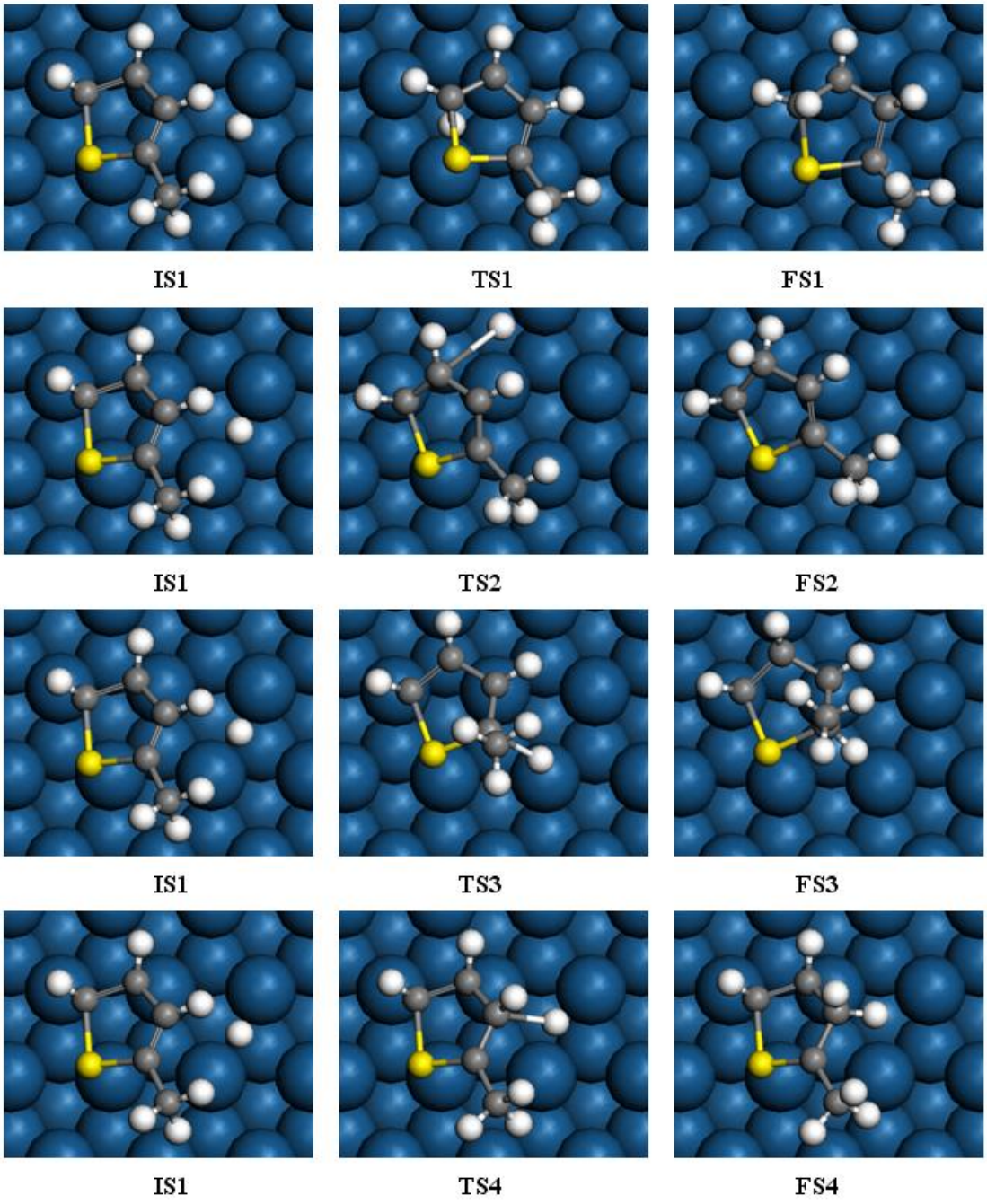

Fig. 4. IS, TS, FS, activation energy and reaction energy (kJ·mol^{-1}) of step 1

Note: FS1: E_a = 167.7; ΔE = –52.2, FS2: E_a = 75.0; ΔE = –8.1

FS3: E_a = 130.9; ΔE = –54.9, FS4: E_a = 187.1; ΔE = 29.7

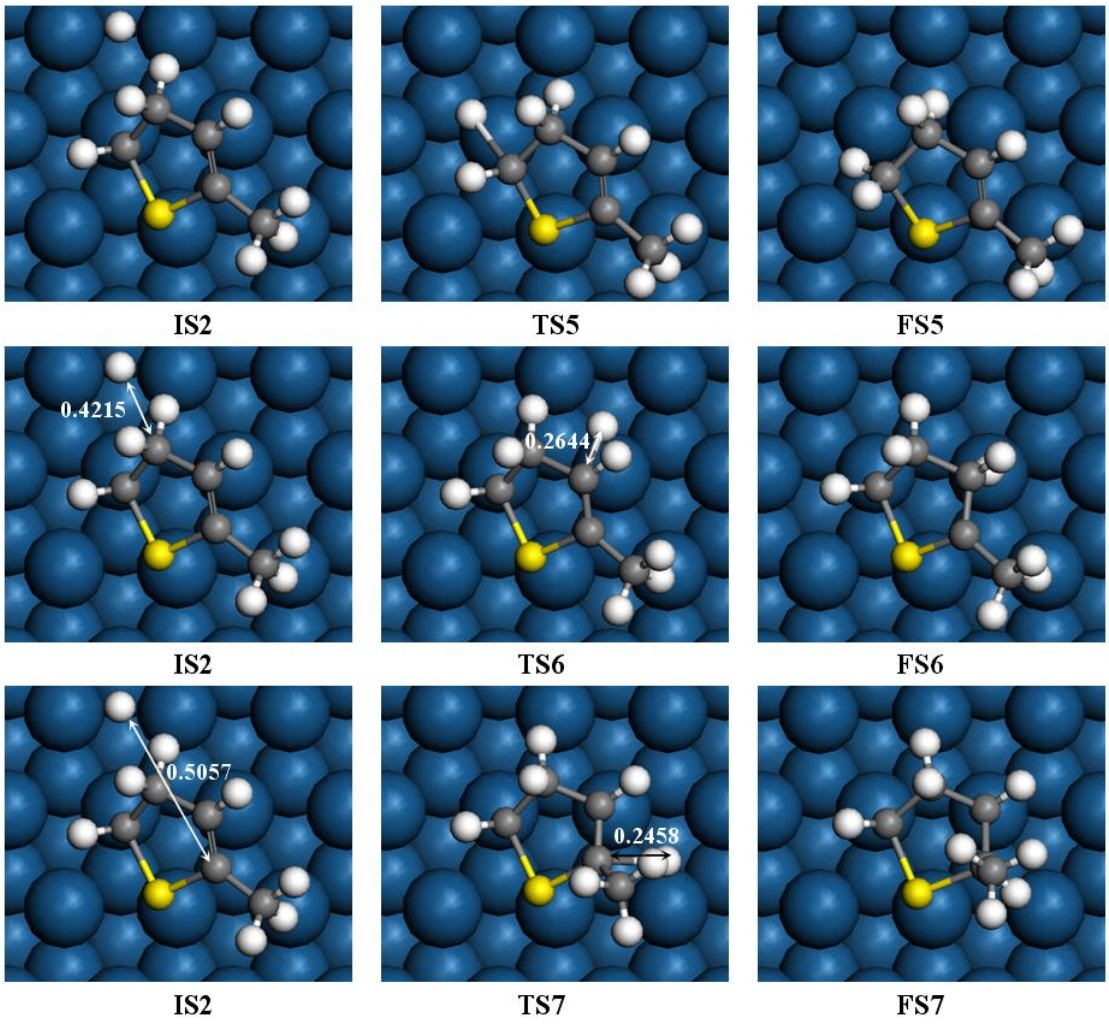

Fig. 5. IS, TS, FS, activation energy, reaction energy (kJ·mol^{-1}) and bond length (nm) of step 2

Note: FS5: E_a = 164.6; ΔE = 11.6, FS6: E_a = 19.5; ΔE = 5.3, FS7: E_a = 109.3; ΔE = 76.4

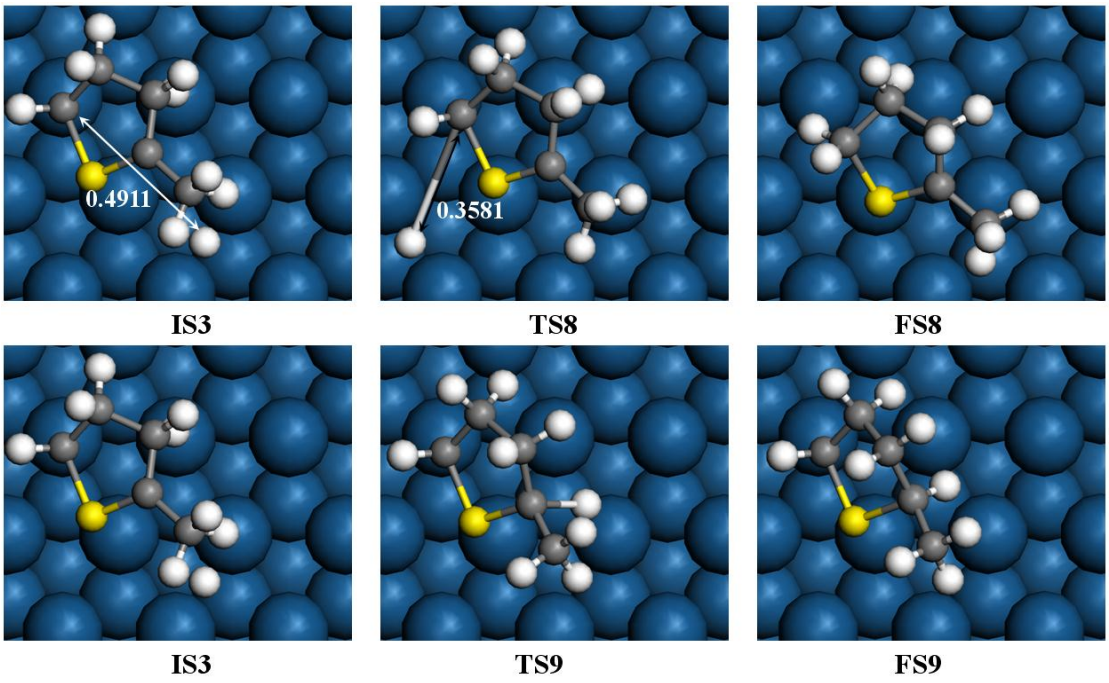

Fig. 6. IS, TS, FS, activation energy, reaction energy (kJ·mol^{-1}) and bond length (nm) of step 3

Note: FS8: E_a = 67.9; ΔE = -102.1, FS9: E_a = 97.3; ΔE = 5.3

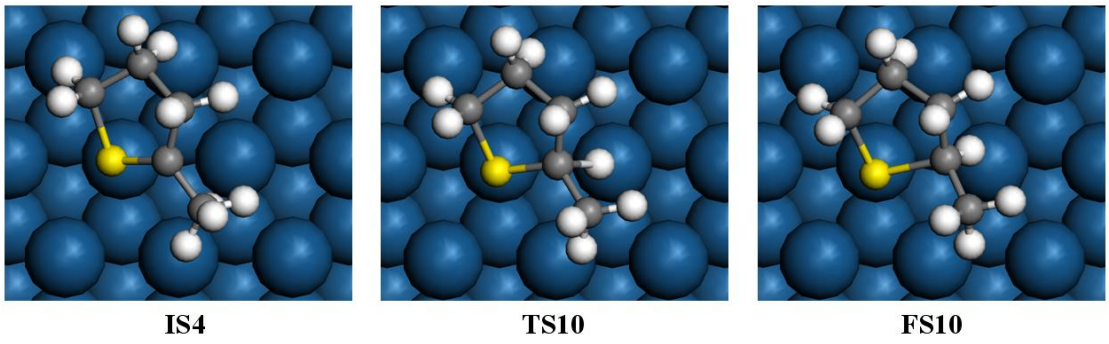

Fig. 7. IS, TS, FS, activation energy and reaction energy (kJ·mol^{-1}) of step 4

Note: FS10: E_a = 112.6; ΔE = –97.0

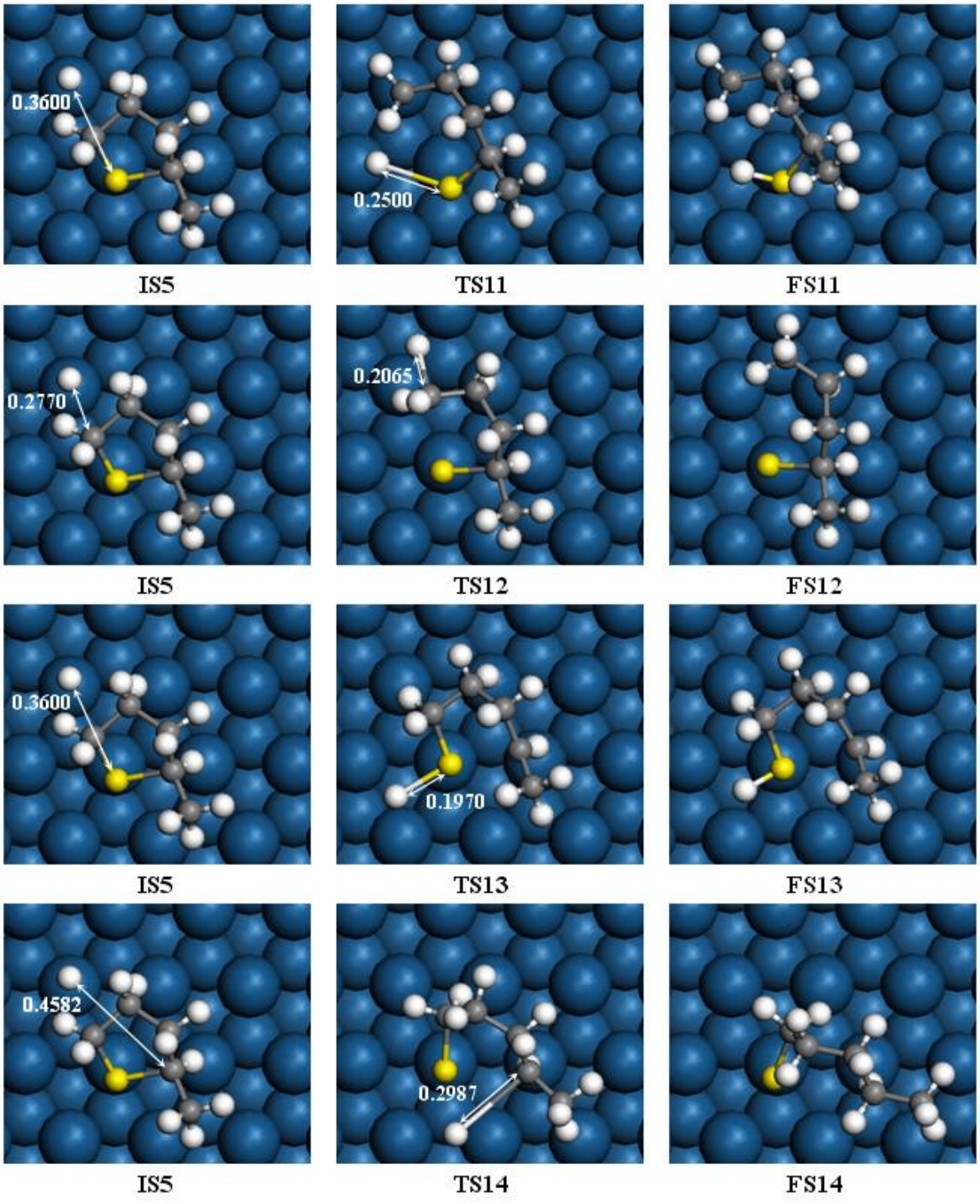

Fig. 8. IS, TS, FS, activation energy, reaction energy (kJ·mol^{-1}) and bond length (nm) of step 5

Note: FS11: E_a =116.9; ΔE = 48.9, FS12: E_a = 388.2; ΔE = 39.3

FS13: E_a = 233.9; ΔE = 138.3, FS14: E_a = 416.0; ΔE = 13.0

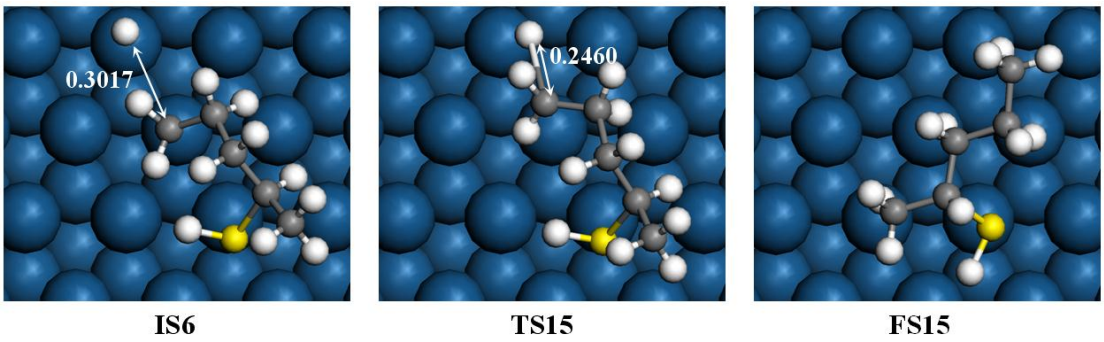

Fig. 9. IS, TS, FS, activation energy, reaction energy (kJ·mol^{-1}) and bond length (nm) of step 6

Note: FS15: E_a =210.8; ΔE = –15.8

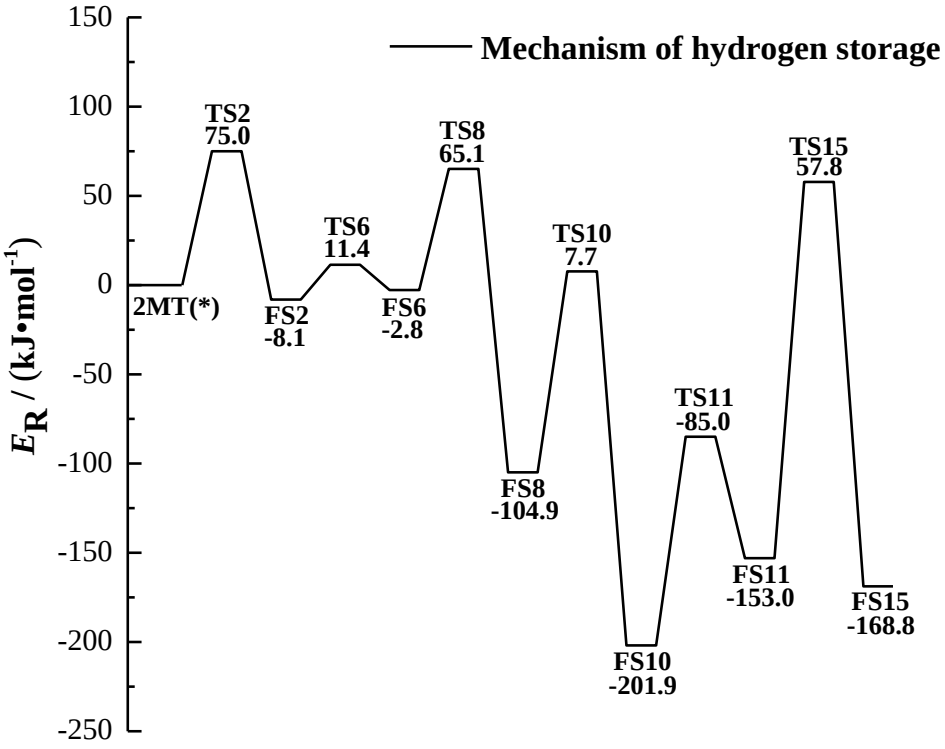

Fig. 10. Sketch for potential relative energy (E_R) of hydrogenation mechanisms on the Pt(111) surface

Theoretical Study on the Adsorption and Hydrogenation Mechanism of 2-Methylthiophene over the Pt(111) Catalyst

SHI Wei(施炜)　NI Zhe-Ming(倪哲明)
XIA Sheng-Jie(夏盛杰)　SU Wei-Ke(苏为科)

The tilt adsorption of 2-methylthiophene molecule on the Pt(111) surface at the top site through the double bond of C_1 and C_2 is the most stable. The dominant channel follows the hydrogenation step of $C_2 \rightarrow C_3 \rightarrow C_1 \rightarrow C_4 \rightarrow S \rightarrow C_1$ to generate the product of pentane-2-thiol. And the storage is almost exothermic, so that reducing the temperature is beneficial to the reaction.